frontiers in Energy Research

REVIEW
published: 06 October 2021
doi: 10.3389/fenrg.2021.759850

Minimum Detectable Activity of Pb-210 in Skull From *In vivo* Measurements: Insights From the Literature

Xiangpeng Meng[1], Yuanyuan Liu[1], Bin Wu[1]*, Jianping Cheng[1], Li Wang[2], Yu Wang[1] and Ning Su[1]*

[1]Key Laboratory of Beam Technology of Ministry of Education, College of Nuclear Science and Technology, Beijing Normal University, Beijing, China, [2]Department of Physics, Beijing Normal University, Beijing, China

To address the urgent need for the retrospective assessment of the health conditions of people with a history of appreciable radon exposure, a novel technique that directly measures the characteristic γ-rays emitted from Pb-210 in the living skull was developed. Since the first pioneering study in 1968, this technique has experienced continued advancement over more than half a century, where the limit of detection of Pb-210 is a common criterion to assess the performance of the measuring devices. However, researchers have defined the limit of detection in assorted ways, and the measurement conditions often greatly differ from study to study, both of which significantly challenge interstudy comparisons and obscure how various factors make their impacts. In this work, we reanalyze the reported results in the literature according to the minimum detectable activity (MDA) defined by Currie and investigate the effects of key elements therein. Firstly, we focus on the reported background count rates and analyze their dependence on detector's energy resolution and active area. Secondly, we turn to the reported calibration factors and conduct analysis in the same manner. Thirdly, we calculate MDA for each study and monitor its dependence on the active area of detector and measurement duration. In the limit of the largest achievable active area (~75000 mm^2), it is found that the asymptotic MDA is approximately 6 (4) Bq and 15 (11) Bq under 30 (60) min measurement using NaI-CsI scintillator and HPGe semiconductor detectors, respectively. Finally, we discuss these asymptotic MDA in the context of estimated Pb-210 activity in the skull resulted from a hypothetical history of radon exposure.

Keywords: Pb-210, MDA, NaI-CsI, HPGe, *in vivo* measurement

OPEN ACCESS

Edited by:
Mingfei Yan,
RIKEN, Japan

Reviewed by:
Rong Zhou,
Sichuan University, China
Ayhan Kara,
Giresun University, Turkey
Qiuju Guo,
Peking University, China

****Correspondence:***
Yuanyuan Liu
yyliu@bnu.edu.cn
Bin Wu
bwu6@bnu.edu.cn

Specialty section:
This article was submitted to Nuclear Energy, a section of the journal Frontiers in Energy Research

Received: *17 August 2021*
Accepted: *20 September 2021*
Published: *06 October 2021*

Citation:
Meng X, Liu Y, Wu B, Cheng J, Wang L, Wang Y and Su N (2021) Minimum Detectable Activity of Pb-210 in Skull From In vivo Measurements: Insights From the Literature. Front. Energy Res. 9:759850. doi: 10.3389/fenrg.2021.759850

INTRODUCTION

Radon (Rn-222) is a rare gas with radioactivity. It is derived from uranium decay series and is widely present in nature. In particular, radon is enriched in basements and mines, where air circulation is commonly poor and the environment is surrounded by soils or rocks that contain high concentrations of uranium (~thousands of Bq/m^3) (Cevik et al., 2010; Cevik et al., 2011; Somlai et al., 2011; Meng et al., 2015; Fijałkowska Lichwa, 2016; Sahu et al., 2016; Sun et al., 2020; Kojo et al., 2021). Once radon is inhaled, the alpha particles emanating from the radon and its daughters inevitably deposit energy in the lungs, thereby causing radiation damage to the lung tissues (Black

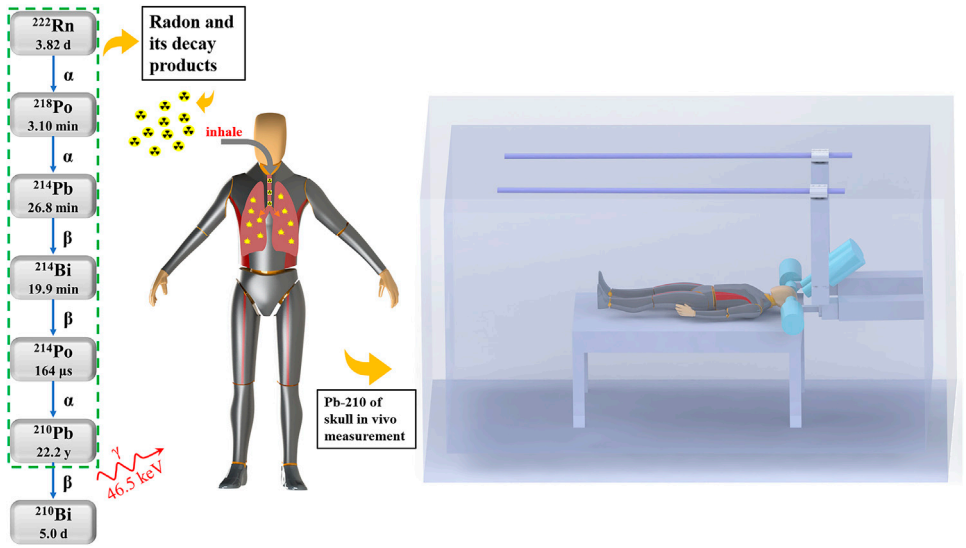

FIGURE 1 | Schematic diagrams of the radon decay chain, inhalation of radon and its decay products, and the Pb-210 *in vivo* measurement device, where four high purity germanium (HPGe) detectors are positioned around the head of a tested person inside the shielding room.

et al., 1968; Blanchard et al., 1969; Wahl et al., 2000; Momcilovic et al., 2001; Pillalamarri et al., 2013). The cumulative effects of such radiation damage from long-term living or working in a high radon environment greatly increase the risk of lung cancer (WHO, 2009). This is arguably the leading reason why the probability of lung cancer among miners is much higher than that of the general public. Accordingly, the World Health Organization (WHO) has listed radon as a class I carcinogen and identified it as the second leading cause of lung cancer, next only to smoking.

It is thus desirable to determine the potential alpha energy exposure (PAEE) of individuals with a history of substantial radon exposure, e.g., miners, so that retrospective assessments of their health conditions can be performed in a timely manner. Currently, the dominant method of reconstructing PAEE relies on two factors, namely radon concentration onsite and the estimated duration of exposure (UNSCEAR, 2019; Tomasek, 2020). For example, the working level month (WLM) represents the cumulative exposure of an individual working 170 h in total in an environment with an emission of 1.3×10^5 MeV potential alpha energy per liter from short-lived daughters of radon (Black et al., 1968; Blanchard et al., 1969). However, this method suffers from large uncertainties because radon activity in the environment often strongly fluctuates over time and locations, the human respiration rate may differ significantly among individuals, and residence time in a high radon environment often depends on subjective recollection, which may considerably deviate from reality (Laurer et al., 1993).

In contrast, reconstructing the cumulative radon intake of a tested person based on the direct measurement of Pb-210 activity in the living skull is a very promising, cutting-edge method. Its scientific basis can be briefly described as follows: Pb-210 is a relatively stable nuclide formed after short-term decay of Rn-222, and its half-life is ~22 years, as shown in **Figure 1**. Since lead is a chemical congener of calcium, its biodynamic characteristics in the human body are very similar to those of Ca (ICRP, 1993; Dantas et al., 2006); hence, the Pb-210 formed from the decay of radon that has been inhaled shall ultimately transport to the bones and distribute evenly among them. In other words, the bones can act as a good "dosimeter" (Laurer et al., 1999), and the activity of Pb-210 contained therein directly reflect individual's cumulative exposure to radon. Among the many bones, the skull has the largest surface area (Estrada et al., 1993), accounting for approximately 13–15% of the total bone mass (ICRP, 1975; Wahl et al., 2000). Moreover, its upper epidermis is relatively thin, and the difference between individuals is small. Therefore, it is the best choice for Pb-210 activity measurement *in vivo* (Cohen et al., 1977).

Admittedly, there are indeed potentially large uncertainties underlying this approach, because there can be assorted sources contributing to the Pb-210 activity in the skull other than radon (Laurer et al., 1999). However, we are strong confident that this approach promises great potential for the following three reasons: Firstly, the associated uncertainty can be reasonably suppressed through carefully setting up the control group for measurements; secondly, the Pb-210 activity originating from other sources becomes trivial comparing to radon when the person of interest had been subject to substantial radon exposure (see Discussion for more details). Thirdly, in many cases, the Pb-210 *in vivo* measurement could be the only viable measure to reconstruct one's radon intake, as the radon concentration may not be available.

In 1968, Eisenbud et al. first verified the feasibility of this idea by directly measuring the characteristic γ-rays emitted by Pb-210 in the living skull of miners (Eisenbud et al., 1969). Following this

pioneering study, the technique of Pb-210 *in vivo* measurements has attracted considerable interests from researchers all around the world and enjoyed continued advancement in the past 50 years (Cohen et al., 1973; Cohen et al., 1977; Zheng et al., 1992; Estrada et al., 1993; Laurer et al., 1993; Scheler et al., 1998; Wahl et al., 2000; Muikku et al., 2003; Dantas et al., 2006; Dantas et al., 2007; Pillalamarri et al., 2013). It is generally consent that the detection of Pb-210 *in vivo* is extremely subject to the background interference because the activity of Pb-210 in the skull is often very low (~10 Bq) (Wahl et al., 2000; Dantas et al., 2007), the branching ratio of γ decay is as low as 4.25%, and the energy of released γ-rays is only 46.5 keV, thereby characterizing poor penetrating capability. Consequently, researchers often adopt the limit of detection to assess the sensitivity of their measuring devices. Nonetheless, throughout the literature, researchers have defined the limit of detection in a variety of ways (Altshuler et al., 1963; Isenhour et al., 1964; Kirkpatrick et al., 2013; Done et al., 2016), which severely compound the interstudy comparison and obscure how various factors make their impacts. To unravel this challenge, we resort to the concept of minimum detectable activity (MDA) defined by Currie (Currie, 1968) and reanalyze the data reported in the literature. The results presented in this work clearly demonstrate how key factors, such as detector's active area and energy resolution, background level, and measurement time, influence MDA and thus shed light on the future direction for further improvement.

The rest of this article is organized as follows: in *MDA Derivation*, we demonstrate the derivation of MDA and identify the critical factors therein; in *Results and Discussion*, we present the key figures from the literature and reanalyze the reported data; we make concluding remarks in *Conclusion*.

MDA DERIVATION

The derivation of MDA was described in detail in Currie's classical article (Currie, 1968), which we briefly recapitulate below. We note that the MDA_{ISO} defined by the ISO standard has also been widely used in many studies (ISO, 2010). Comparing with Currie's MDA, the ISO standard takes the uncertainty in the calibration factor into account. In this regard, MDA_{ISO} is admittedly more rigorous. Nonetheless, there are two reasons for adopting MDA_{Currie} in our study: First, among the studies focusing on Pb-210 *in vivo* measurement, the uncertainty in the calibration factor was mostly not considered and thus not documented in the publication. Consequently, it become impractical to employ MDA_{ISO} in our study. Second, it has been pointed out by Kirkpatrrick that two definitions of MDA yield quite similar results when the uncertainty in the calibration factor is smaller than 10% (Kirkpatrrick et al., 2013). Because it is common to employ an anthropomorphic phantom enclosing Pb-210 with activity up to 5,000 Bq for calibration, the resultant uncertainty in the calibration factor should be fairly small. Hence, we consider two definitions of MDA should lead to essentially the same results.

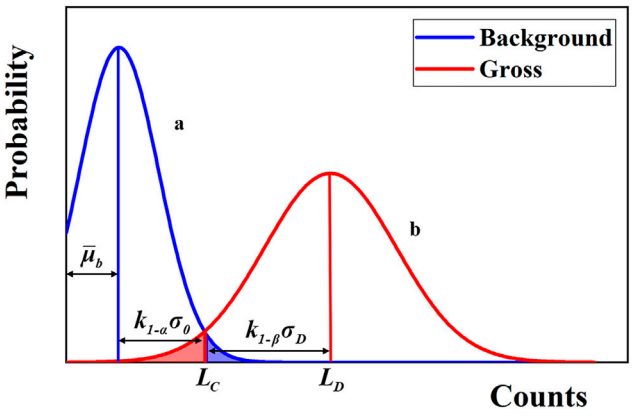

FIGURE 2 | Schematic diagram of two types of errors. The Gaussian-shaped curves in blue and red represents the probability distributions of counting statistics for measurements on background and sample (under the same background), respectively. The shaded parts denote the probability of the first (blue) and second (red) type of errors, respectively.

Let's imagine a general scenario, where a surveyor needs to rely on a certain measurement system to detect radiation from a sample with unknown radioactivity. First, the surveyor needs to determine the background level under the measurement conditions. Because the processes of nuclear decay, particle transportation, and radiation detection all characterize random features, the results of each measurement differ statistically. By measuring the background several times with equal measurement duration of t_b, the arithmetic average of multiple measurement results and their variance can be computed, which are denoted $\bar{\mu}_b$ and $\sigma_{\bar{\mu}_b}$, respectively. With these statistical samplings, one can consider the average background level is approximately $\bar{\mu}_b$ and calculate its standard deviation $\sigma_b$as follows:

$$\sigma_b = \sqrt{\bar{\mu}_b + \sigma_{\bar{\mu}_b}^2} \tag{1}$$

where it is assumed that the background statistics obey the Poisson distribution, and the principle of error propagation is used.

In the next step, the surveyor needs to perform measurements under the presence of the sample with measurement duration of t_s and analyze if it contains radioactivity. Two types of errors may occur. The first type of error is misjudging that the sample is radioactive whereas in reality it isn't. The critical level L_C is a threshold set to avoid such errors under a certain confidence level. To be more specific, it equals to the upper limit of the background count under the confidence of $1-\alpha$, as shown in **Figure 2**, and can be expressed as below:

$$L_C = \bar{\mu}_b + k_{1-\alpha}\sigma_b \tag{2}$$

where $k_{1-\alpha}$ represents the abscissa corresponding to the confidence interval $1-\alpha$ on the standard normal distribution. The second type of error is misjudging that the sample is not radioactive whereas in reality it is. The detection limit L_D is a threshold set to avoid such errors under a certain confidence level. In the similar manner, it equals to the lower limit of the total count (including background and sample) under the $1-\beta$

TABLE 1 | Key features from the studies focusing on Pb-210 *in vivo* measurements.

Researchers (publication year)	Detector			Structure of shielding room	N_b (cps)	v (cps/Bq)	t_s (min)	*: L_C' #: *LLD* +: *MDA* (Bq)
	Type	A (mm^2)	ROI (keV)					
Eisenbud et al. (1969)	NaI-CsI	32,429	30-70	15.24 cm steel	0.749	3.15×10^{-3}	10	31.08*
Cohen et al. (1973)	NaI-CsI	36,483	30-60	15.24 cm steel followed by graded-Z lining (Pb, Cd, Cu)	0.519	4.50×10^{-3}	100	4.81*
Cohen et al. (1977)	NaI-CsI	54,724	30-60	16 cm steel followed by graded-Z lining (Pb, Cd, Cu)	1.37	5.59×10^{-3}	100	6.29*
Zheng et al. (1992)	NaI-CsI	12,272	30-65	10 cm Pb	0.100	1.50×10^{-3}	N/A	N/A
Estrada and Laurer (1993)	NaI-CsI	54,724	23.15-66.13	16 cm steel followed by graded-Z lining (Pb, Cd, Cu)	0.832	6.17×10^{-3}	90	2.8*
Scheler et al. (1998)	HPGe	8,000	N/A	15 cm steel followed by graded-Z lining (Pb, Cu)	N/A	N/A	120	5.1#
Wahl et al. (2000)	HPGe	24,400	45.75-47.25	N/A	0.075	2.3×10^{-3}	120	6.7+
Haninger et al. (2002)	HPGe	15,703	45.75-47.25	N/A	0.0339	1.9×10^{-3}	120	5.2#
Dantas et al. (2007)	HPGe	8,000	46.1-46.9	15 cm steel followed by graded-Z lining (Pb, Cd, Cu)	0.0109	6.54×10^{-4}	60	6.2*

confidence level, as shown in **Figure 2**, and can be expressed as follows:

$$L_D = \left(\mu_S + \overline{\mu}_b\right) - k_{1-\beta}\sqrt{\mu_S + \sigma_b^2} \tag{3}$$

where μ_s represents the actual net count resulted from the sample, and $k_{1\text{-}\beta}$ has the same meaning as $k_{1-\alpha}$. Setting $\mu_s = L_D$ and $\alpha = \beta$ leads to the following equation:

$$L_D = k_{1-\alpha}^2 + 2k_{1-\alpha}\sqrt{\overline{\mu}_b + \sigma_{\overline{\mu}_b}{}^2} \tag{4}$$

Finally, MDA is defined by converting the decision limit L_D through the calibration factor ν, namely:

$$MDA = \frac{L_D}{t_s \cdot \nu} = \frac{L_D}{t_s \eta \varepsilon} = k_{1-\alpha}^2 + 2k_{1-\alpha}\frac{\sqrt{\overline{\mu}_b + \sigma_{\overline{\mu}_b}{}^2}}{t_s \eta \varepsilon} \tag{5}$$

where η is the probability of the sample emitting the characteristic γ-ray to be measured in one decay (*i.e.*, branching ratio), and ε is the detection efficiency of the γ-rays by the measuring system. Note that the calibration factor ν equals to the product of η and ε. MDA thus represents the minimum activity of the sample that can be recognized by the measuring device with confidence level of $k_{1-\alpha}$ through counting the characteristic γ-rays emanating from the sample under the measurement conditions including duration, detection efficiency, and background.

It should be noted that t_b can be different from t_s, but then the average and standard deviation of the background count need to be normalized according to t_s. In addition, researchers often use single measurement to estimate the background and set the confidence level to be 95%. Under these circumstances, $\sigma_{\overline{\mu}_b{}^2 = \overline{\mu}_b}$, and $k_{1-\alpha} = 1.64$; finally, the following simplified expression can be obtained:

$$MDA = \frac{k_{1-\alpha}^2 + 2k_{1-\alpha}\sqrt{2\overline{\mu}_b}}{t_s \eta \varepsilon} = \frac{2.71 + 4.65\sqrt{\overline{\mu}_b}}{t_s \eta \varepsilon} \tag{6}$$

Equation 6 is arguably the most commonly used expression in the field of radiation detection.

In addition to the MDA listed above, researchers also employed other quantities to evaluate the limit of detection including L_C' and *LLD* (Altshuler et al., 1963), which are shown below:

$$L_C' = \frac{k_{1-\alpha}\sqrt{2\overline{\mu}_b}}{t_s \nu} \tag{7}$$

$$LLD = \frac{2k_{1-\alpha}\sqrt{2\overline{\mu}_b}}{t_s \nu} \tag{8}$$

The application of these various measures for limit of detection apparently causes great difficulties for comparisons among studies as shown next.

RESULTS AND DISCUSSION

Table 1 summarizes the key features from the studies focusing on Pb-210 *in vivo* measurements (Eisenbud et al., 1969; Cohen et al., 1973; Cohen et al., 1977; Zheng et al., 1992; Estrada et al., 1993; Scheler et al., 1998; Wahl et al., 2000; Haninger et al., 2002; Dantas et al., 2007), including characteristics of detectors, measurement time t_s, calibration factor ν, and background count rate N_b.

It is first noticed that two types of detectors were commonly employed, namely NaI-CsI scintillator detectors and high-purity germanium (HPGe) semiconductor detectors. Because they characterize drastically distinct energy resolution, the region-of-interest (ROI) and its corresponding width in the measurement spectrum are dramatically different. To be more precise, the full width at the half maximum (FWHM) of the scintillator detector is ~9 keV at 46.5 keV, and that of the semiconductor detector is ~0.6 keV at 46.5 keV. As a result, the width of ROI for NaI-CsI detector is approximately 40 keV, whereas that for HPGe detector is roughly 2 keV. Besides energy resolution, two types of detectors also differ considerably in active area A; it is common that scintillator detectors often characterize much larger active area than HPGe detectors. On

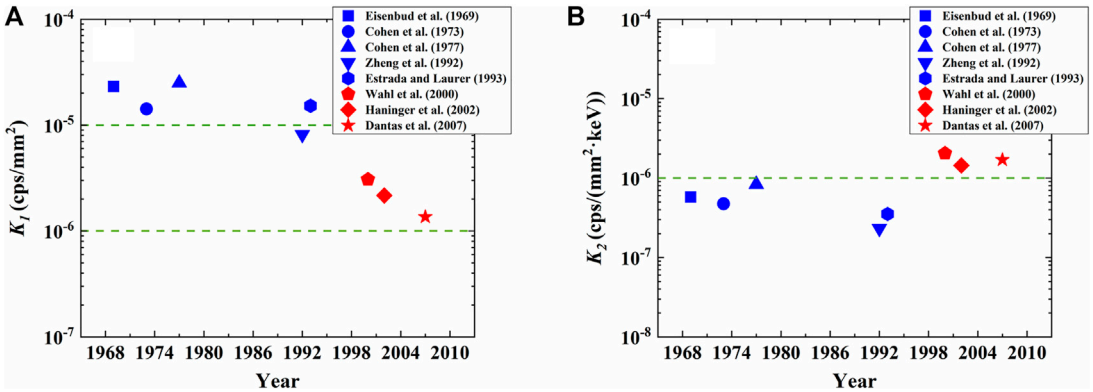

FIGURE 3 | Dependence of background count rate on active area and width of ROI for various studies. In panel **(A)**, K_1 represents the background count rate per active area; in panel **(B)**, K_2 represents background count rate per active area per ROI energy.

average, the active area for the studies employing NaI-CsI detectors is 4.4×10^4 mm^2 while that for HPGe detectors is 2.8×10^4 mm^2.

The width of ROI and active area are two critical factors that affect the limit of detection. Under a fixed level of background, it can be understood that a wider ROI would necessarily lead to a higher background count rate N_b and equivalently the background count $\overline{\mu}_b$ within the measurement duration. In this sense, a smaller ROI resulted from a finer energy resolution is more advantageous for lowering MDA. In contrast, the active area influences the limit of detection in a more complex way. On the one hand, a larger active area would improve the efficiency in detecting the targeted γ-rays, because the solid angle spanned by detector towards the skull is wider; on the other hand, it can also increase the counts on the background in the same way. We analyze these factors in more detail in *Analysis of Background Count Rate* N_b and *Analysis of the Calibration Factor* v.

In addition to the detector factors, the duration of measurement also plays a considerable role. We see the measurement time varies widely among studies and is commonly set to more than 1 h. Furthermore, as shown in **Table 1**, researchers also employed various quantities to measure the limit of detection. In *Comparison of MDA Among Studies*, we rely on the reported data and unify these measures according to the MDA derived in the prior section. Moreover, we demonstrate the evolution of MDA under the variation of detector's active area and the length of measurement.

Analysis of Background Count Rate N_b

Equation 6 clearly indicates that MDA largely depends on the radiation background. **Table 1** shows that the background count rate N_b widely differs between the studies employing NaI-CsI and HPGe detectors, which is on the order of $\sim 10^{-1}$ and $\sim 10^{-2}$ cps, respectively. Such a difference is attributable to three factors, namely inherent background level, width of the ROI, and active area of detectors. We assess the influence of each factor below.

First, we normalize the background count rate by the active area of detectors as follows,

$$K_1 = N_b / A \tag{9}$$

K_1 thus represents the background count rate per active area of the detector, and the results are depicted in **Figure 3A**. It is directly recognizable that the K_1 from various studies are again divided into two groups based on the types of detectors, where K_1 for NaI-CsI detectors illustrated in blue is much higher than that of the HPGe detector shown in red, yielding the magnitude of $\sim 10^{-5}$ cps/mm^2 and $\sim 10^{-6}$ cps/mm^2, respectively.

We next normalize the K_1 by the width of ROI (ΔE) as follows,

$$K_2 = K_1 / \Delta E \tag{10}$$

K_2 thus typifies the background count rate per unit area of the detector per ROI energy. It should be noted that in order to create a low radiation background environment for *in vivo* measurement, a shielding room made of thick metallic wall is commonly employed, as shown in **Figure 1** and **Table 1**. Therefore, K_2 mainly reflects the background level inside the shielding room, because the characteristic features that are unique to different types of detectors are mostly removed. The results shown in **Figure 3B** suggest that K_2 from various studies is very close, characterizing the magnitude of $\sim 10^{-6}$ cps/(mm^2·keV). This observation indicates that the background levels inside the shielding rooms are approximately the same. This is because a ~15 cm thick steel or ~10 cm Pb can attenuate the γ-rays from environment by 99% and the benefit of further increasing wall's thickness is very limited (Verplancke, 1992; Cannizzaro et al., 1997; Mrdja et al., 2019). In this regard, it would be necessary to resort to other routes to further suppress background, such as active shielding through muon veto techniques (Semkow et al., 2002).

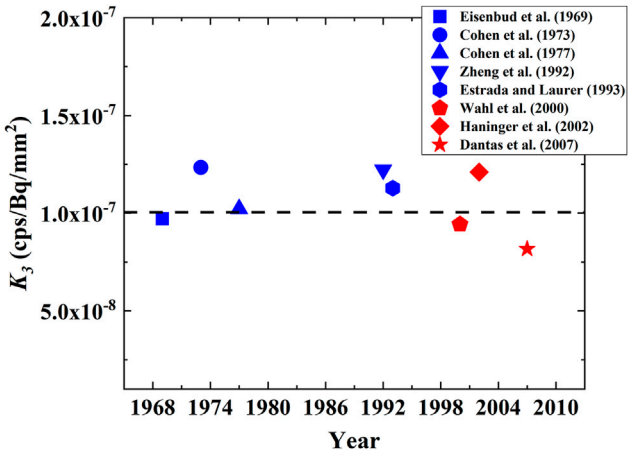

FIGURE 4 | Dependence of efficiency calibration factor on the active area of detector. K_3 represents detection efficiency per active area.

Analysis of the Calibration Factor *v*

In addition to the background count rate, the MDA is also strongly dependent on the detection efficiency through the calibration factor v. Because the energy of the γ-rays emitted by Pb-210 is low, only 46.5 keV, the intrinsic efficiency of the NaI-CsI (Leone et al., 2011; Meng et al., 2021) and HPGe detectors (Pillalamarri et al., 2019; Turko et al., 2020) in this energy range is very high, close to 100%. Therefore, the detection efficiency here refers to the absolute detection efficiency, which is mainly determined by the active area of the detector.

To assess the influence of active area, we follow the same normalization method to define the detection efficiency per active area of the detector, as listed below:

$$K_3 = v/A \tag{11}$$

The results shown in **Figure 4** indicate that K_3 are approximately the same across various studies, showing the magnitude of $\sim 10^{-7}$ cps/(Bq^{-1}·mm^{-2}). This observation indicates that there is no significant difference between NaI-CsI and HPGe detectors in the capability of detecting Pb-210.

Comparison of MDA Among Studies

In this section, we seek to make a fair interstudy comparison by employing Currie's MDA as the unanimous criterion of quantifying the limit of detection and to evaluate the dependence of MDA on the active area and measurement duration. We introduce K_1 and K_3 defined in prior sections into **Eq. 6** and assume a 95 % confidence level, which gives the following expression,

$$MDA = \frac{2.71 + 4.65\sqrt{K_1 \cdot A \cdot t}}{t \cdot K_3 \cdot A} \tag{12}$$

The calculation results are illustrated in **Figure 5**, where panel (A) corresponds to 30 min measurement while panel (B) is for 1 h measurement; furthermore, each line denotes different studies and reflects the evolution of MDA in response to the variation of active area of detectors; in addition, the solid symbols represent the active areas reported in the original studies.

Firstly, the lines corresponding to NaI-CsI detectors generally characterize higher MDA than those employing HPGe detectors under the same active area and measurement duration. Secondly, the lines are self-similar showing steep drop in the beginning and then gradually saturate as active area A continuously increases. Qualitatively speaking, when the active area of detectors has reached certain size, e.g. ~25,000 mm^2, lowering MDA by further expanding the active area of detectors becomes highly inefficient. Note that the effective surface area of the head excluding the section connected to the neck is estimated to be ~75,000 mm^2, based on which one can infer the lowest MDA achievable for each study. Under the 30 min measurement, the lowest achievable MDA using NaI-CsI detectors and HPGe detectors are ~15 and ~6 Bq, respectively, while under 1 h measurement, they are ~11 and ~4 Bq, respectively. Increasing the measurement time indeed leads to the decrease in MDA, but

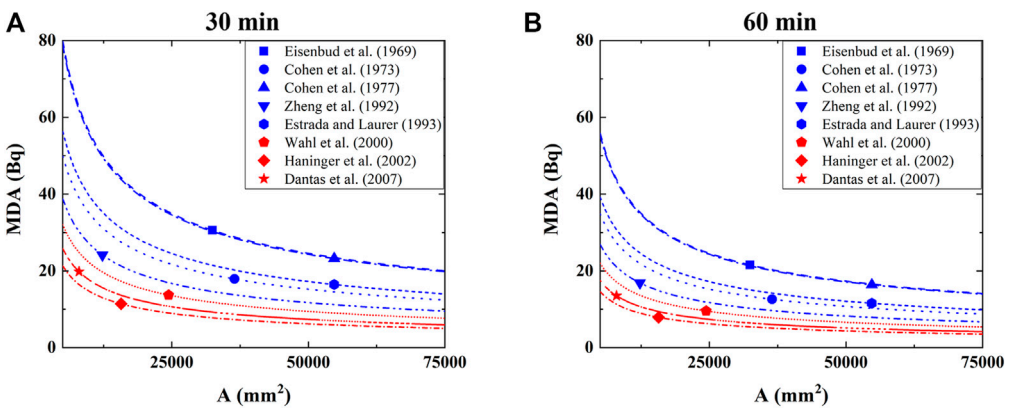

FIGURE 5 | The dependence of MDA on the active area of detector and measurement time, where the filled symbols represent the active areas reported in the original studies.

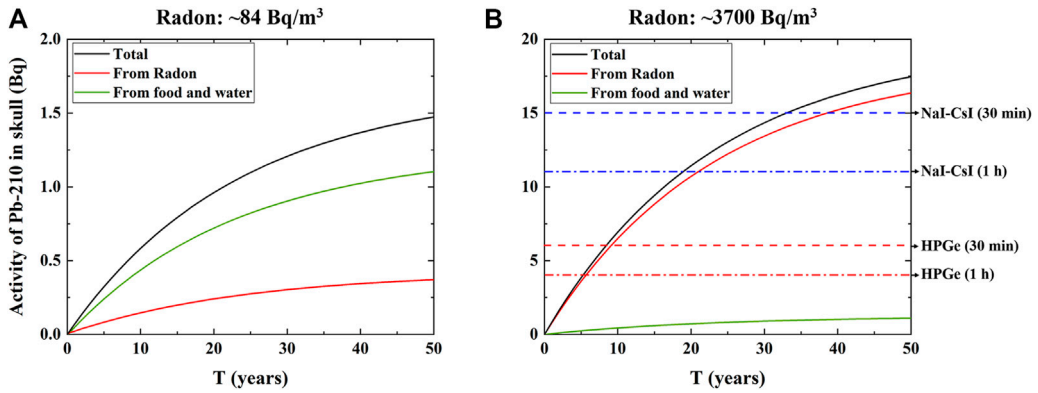

FIGURE 6 | Estimated Pb-210 activity in skull originating from various source as a function of exposure time. In **(A)**, the data are extracted from Laurer et al. (1999), where the radon concentration is estimated to be ~84 Bq/m^3; based on the same model, in conjunction with the assumed radon concentration of 3,700 Bq/m^3, the Pb-210 activity from various sources are presented in **(B)** comparing to the asymptotically achievable MDAs using NaI-CsI (blue) and HPGe (red) detectors under the measurement time of 30 min (dashed) and 1 h (dot-dashed).

the benefit is not so significant. Moreover, withholding a person in the testing position for too long would necessarily place considerable mental as well as physical stress to that person. Therefore, unless absolutely necessary, the duration should not exceed ~30 min for each measurement. Interestingly, Estrada and Laurer employed multiple separated 30 min measurements (Estrada et al., 1993), which we consider is a wise practice to lower MDA.

Discussion

It is informative to consider the MDA in the context of potential Pb-210 activity in the skull of individuals, who had a substantial radon exposure history, denoted A_{skull}. To this end, we refer to the model by Eisenbud et al., which assumes that the tested person is subject to a continuous exposure to radon with fixed concentration. Mathematically, it is shown below,

$$\mathrm{A}_{skull} = \frac{A_P}{\lambda_{eff}} \cdot W \cdot \left(1 - \exp\left(-\lambda_{eff} \cdot T\right)\right) \cdot f \qquad (13)$$

where A_p is the activity of Pb-210 deposited in skull per WLM, λ_{eff} is the biodynamic half-life of Pb-210 in bone, W is the average exposure of workers per month in terms of WLM, T is time since the first exposure, and f is the weight fraction of skull in bones. Following references (Eisenbud et al., 1969; Laurer et al., 1999), we assign A_p = 0.31 Bq/WLM, λ_{eff} = 16 years, and f = 15%. Furthermore, for simplicity, we assume the decays of radon and daughters are always in equilibrium, and that the individual has been maintaining 8 h per day in the environment with fixed radon concentration.

One can imagine that there can be a variety of sources leading to Pb-210 activity other than radon, such as diet. Laurer et al. has reported the estimation on the contributions from these sources (Laurer et al., 1999), which we replot in **Figure 6A**; the green line represents the contribution from food and water, while the red line denotes that from radon. We have successfully repeated the prediction on radon with the model listed in **Eq. 13**, and found that the radon concentration is as low as 84 Bq/m^3, which is much lower than the concentration commonly studied in similar works. Therefore, by assuming that the radon concentration is 3,700 Bq/m^3 instead, we replot predicted Pb-210 activity in the skull as a function of exposure time in **Figure 6B**, where the contribution from sources other than radon are copied from **Figure 6A**. It is evident that the radon becomes the dominant source of Pb-210 activity in this scenario.

For comparison, the asymptotically achievable MDA using NaI-CsI (blue) and HPGe (red) detectors under the measurement time of 30 min and 1 h are superimposed as dashed and dot-dashed lines, respectively. Note that the active area of detectors is assumed to be 75,000 mm^2.

Under 30 min measurement, the device relying on NaI-CsI detectors can barely detect the presence of Pb-210 activity for individuals who had more than 30 years of exposure; by extending the measurement time to 1 h, those with more than 20 years of exposure can be recognized. In contrast, by relying on the HPGe detectors, the individuals, who had more than 5–8 years of exposure, can be identified. Therefore, a lower MDA resulted from employing HPGe detectors instead of NaI-CsI detectors can lead to a much earlier recognition of heavy radon exposure by 10–20 years, which is critical for retrospective assessment on lung cancer risks in a timely manner.

CONCLUSION

In this work, we refer to the studies focusing on the Pb-210 *in vivo* measurements and reanalyze the reported data therein to understand how several key factors influence the limit of detection.

Firstly, we focus on the reported background count rates and analyze their dependence on detector's energy resolution and active area. It is found that the background level inside the shielding room of respective studies is almost the same, which

can be rationalized by the saturating capability of metallic walls in suppressing the background through attenuating environmental γ-rays. It is largely due to difference in detector's energy resolution and active area that leads to the considerable differences in background count rates across various studies.

Secondly, we turn to the reported calibration factors and conduct analysis in the same manner. It is found that the detection efficiency is linearly dependent on the active area and is independent on the type of detectors.

Thirdly, we calculate MDA for each study and demonstrate its dependence on the active area of detector and measurement duration. In the limit of the largest achievable active area (~75,000 mm^2), it is found that the asymptotic MDA is approximately 6 (4) Bq and 15 (11) Bq under 30 (60) min measurement using NaI-CsI scintillator and HPGe semiconductor detectors, respectively.

Finally, we discuss these asymptotic MDA in the context of model-estimated Pb-210 activity in the skull resulted from a hypothetical history of radon exposure. It is suggested that a lower MDA would be beneficial to recognize an individual's radon exposure in an earlier stage, which is critical for retrospective assessment on lung cancer risks in a timely manner.

AUTHOR CONTRIBUTIONS

XM conducted the research and wrote the paper, YL designed the research, BW supervised the study and co-wrote the paper, JC provided guidance throughout the research, LW raised valuable questions that helps improving the paper, YW and NS provided good suggestions for data analysis.

FUNDING

This work is supported by the Central University Basic Scientific Research Business Expenses Special Funds under the project name of Research on Applied Physics under Low Radiation Background (Grant No. 2018NTST07) and 2021 Nuclear and Radiation Safety Technic Evaluation Project, Ministry of Ecology and Environment (NSCCG 2021-052).

REFERENCES

Altshuler, B., and Pasternack, B. (1963). Statistical Measures of the Lower Limit of Detection of a Radioactivity Counter. *Health Phys.* 9, 293–298. doi:10.1097/00004032-196303000-00005

Black, S. C., Archer, V. E., Dixon, W. C., and Saccomanno, G. (1968). Correlation of Radiation Exposure and lead-210 in Uranium Miners. *Health Phys.* 14 (2), 81–93. doi:10.1097/00004032-196802000-00001

Blanchard, R. L., Archer, V. E., and Saccomanno, G. (1969). Blood and Skeletal Levels of 210Pb-210Po as a Measure of Exposure to Inhaled Radon Daughter Products. *Health Phys.* 16 (5), 589–596. doi:10.1097/00004032-196905000-00006

Cannizzaro, F., Greco, G., Raneli, M., Spitale, M. C., and Tomarchio, E. (1997). Study of Background Characteristics of a Low-Level HPGe Spectrometer with Passive Shielding in Various Configurations. *Nucl. Instrum. Meth. A.* 390 (1), 167–174. doi:10.1016/S0168-9002(97)00313-6

Cevik, U., Damla, N., Kobya, A. I., Celik, A., and Kara, A. (2010). Radiation Dose Estimation and Mass Attenuation Coefficients of marble Used in Turkey. *Ann. Nucl. Energ.* 37 (12), 1705–1711. doi:10.1016/j.anucene.2010.07.011

Cevik, U., Kara, A., Celik, N., Karabidak, M., and Celik, A. (2011). Radon Survey and Exposure Assessment in Karaca and Çal Caves, Turkey. *Water Air Soil Pollut.* 214, 461–469. doi:10.1007/s11270-010-0437-6

Cohen, N., Jaakkola, T., and Wrenn, M. E. (1973). Lead-210 Concentrations in the Bone, Blood and Excreta of a Former Uranium Miner. *Health Phys.* 24 (6), 601–609. doi:10.1097/00004032-197306000-00001

Cohen, N., Spitz, H. B., and Wrenn, M. E. (1977). Estimation of Skeletal burden of "Bone-Seeking" Radionuclides in Man from *In Vivo* Scintillation Measurements of the Head. *Health Phys.* 33, 431–441. doi:10.1097/00004032-197711000-00009

Currie, L. A. (1968). Limits for Qualitative Detection and Quantitative Determination. Application to Radiochemistry. *Anal. Chem.* 40, 586–593. doi:10.1021/ac60259a007

Dantas, A. L. A., Dantas, B. M., and Lipsztein, J. L. (2006). A Method for Analyzing Low Statistics High Resolution Spectra from 210Pb in Underground Coal Miners from Brazil. *J. Radioanal. Nucl. Chem.* 269 (2), 435–439. doi:10.1007/s10967-006-0404-2

Dantas, A. L. A., Dantas, B. M., Lipsztein, J. L., and Spitz, H. B. (2007). *In Vivo* measurements of 210Pb in Skull and Knee Geometries as an Indicator of Cumulative 222Rn Exposure in a Underground Coal Mine in Brazil. *Radiat. Prot. Dosimetry* 125 (1-4), 568–571. doi:10.1093/rpd/ncl387

Done, L., and Ioan, M.-R. (2016). Minimum Detectable Activity in Gamma Spectrometry and its Use in Low Level Activity Measurements. *Appl. Radiat. Isot.* 114, 28–32. doi:10.1016/j.apradiso.2016.05.004

Eisenbud, M., Laurer, G. R., Rosen, J. C., Cohen, N., Thomas, J., and Hazle, A. J. (1969). *In Vivo* measurement of lead-210 as an Indicator of Cumulative Radon Daughter Exposure in Uranium Miners. *Health Phys.* 16 (5), 637–646. doi:10.1097/00004032-196905000-00011

Estrada, J. J. S., and Laurer, G. R. (1993). A Method to Obtain Subject Background for Low-Level *In Vivo* Measurements of the Head. *Health Phys.* 65 (3), 306–312. doi:10.1097/00004032-199309000-00010

Fijałkowska–Lichwa, L. (2016). Extremely High Radon Activity Concentration in Two Adits of the Abandoned Uranium Mine 'Podgórze' in Kowary (Sudety Mts., Poland). *J. Environ. Radioactivity* 165, 13–23. doi:10.1016/j.jenvrad.2016.08.016

Haninger, T., Wahl, W., Salonen, L., Rahola, T., Kucheida, D., and Roth, P. (2002). *In Vivo* measurements on the Human Skull for Retrospective Assessment of Individual Intakes of Natural Radionuclides. *Int. Congress Ser.* 1225, 95–100. doi:10.1016/S0531-5131(01)00539-8

ICRP (1993). Age-dependent Doses to Members of the Public from Intake of Radionuclides: Part 2. Ingestion Dose Coefficients. A Report of a Task Group of Committee 2 of the International Commission on Radiological Protection. *Ann. ICRP* 23 (3-4), 1–167.

ICRP (1975). *Report of the Task Group on Reference Man*, 23. Oxford: ICRP Publication. Pergamon Press.

Isenhour, T. L., and Morrison, G. H. (1964). A Computer Program to Optimize Times of Irradiation and Decay in Activation Analysis. *Anal. Chem.* 36 (6), 1089–1092. doi:10.1021/ac60212a040

ISO (2010). *ISO 11929 Determination of the Characteristic Limits (Decision Threshold, Detection Limit and Limits of the Confidence Interval) for Measurements of Ionizing Radiation - Fundamentals and Application*. Geneva.

Kirkpatrick, J. M., Venkataraman, R., and Young, B. M. (2013). Minimum Detectable Activity, Systematic Uncertainties, and the ISO 11929 Standard. *J. Radioanal. Nucl. Chem.* 296 (2), 1005–1010. doi:10.1007/s10967-012-2083-5

Kojo, K., Laine, J.-P., Turtiainen, T., and Kurttio, P. (2021). Radon in Finnish Underground Mines 2011-2019. *J. Radiol. Prot.* doi:10.1088/1361-6498/ac08f0

Laurer, G. R., Estrada, J. J. S., and Cohen, N. (1999). Lung Exposure from Inhalation of Radon Progeny. *Health Phys.* 76 (4), 380–387. doi:10.1097/00004032-199904000-00005

Laurer, G. R., Gang, Q. T., Lubin, J. H., Yao, J., Kan, C. S., Xian, Y. S., et al. (1993). Skeletal 210Pb Levels and Lung Cancer Among Radon-Exposed Tin Miners in Southern China. *Health Phys.* 64 (3), 253–259. doi:10.1097/00004032-199303000-00003

Leone, D., and Breustedt, B. (2011). Simulation of Phoswich Detectors Using MCNPX and EGSNRC. *Radiat. Prot. Dosimetry* 144 (1-4), 402–406. doi:10.1093/rpd/ncq507

Meng, D., Xi, P. P., Ma, Y. H., Shen, F., Fu, C. M., and Zhang, Z. L. (2015). Measurement of ^{222}Rn and its Decay Daughters in Uranium Mines. *Radiat. Prot.* 35 (3), 180–187.

Meng, X., Liu, Y., Wu, B., Cheng, J., Wang, L., Wang, Y., et al. (2021). Assessment of Radiation Background Suppression Using Phoswich Detectors for *In Vivo* Pb-210 Measurements: A Simulation Study. *Nucl. Techn.*, 1–8. doi:10.1080/00295450.2021.1945358

Momčilović, B., Alkhatib, H. A., Duerre, J. A., Cooley, M., Long, W. M., Harris, T. R., et al. (2001). Environmental lead-210 and Bismuth-210 Accrue Selectively in the Brain Proteins in Alzheimer Disease and Brain Lipids in Parkinson Disease. *Alzheimer Dis. Associated Disord.* 15 (2), 106–115. doi:10.1097/00002093-200104000-00012

Mrdja, D., Bikit, K., Bikit, I., Slivka, J., Nemes, T., Nikolov, J., et al. (2019). Optimization of the HPGe Detector Passive Shields by Monte-Carlo Simulations. *Nucl. Instr. Methods Phys. Res. Section A: Acc. Spectrometers, Detectors Associated Equipment* 929, 76–83. doi:10.1016/j.nima.2019.03.041

Muikku, M., Rahola, T., Pusa, S., Salonen, L., Wahl, W., Roth, P., et al. (2003). Estimation of Human Exposure to Natural Radionuclides by Using *In Vivo* Skull Measurements. *Radiat. Prot. Dosimetry* 105 (1-4), 615–618. doi:10.1093/oxfordjournals.rpd.a006313

Pillalamarri, I., and Jagam, P. (2019). A Solution for 40K Interference from K Internal to the Human Body, in an Underground High Sensitivity Whole Body Counter at the Waste Isolation Pilot Plant, Carlsbad, NM, USA. *Journal of Radiation Research and Applied Sciences* 10 (4), 320–326. doi:10.1016/j.jrras.2017.07.004

Pillalamarri, I., Jagam, P., and Lykken, G. I. (2013). Internal Dosimetry of 210Pb in the Human Cranium: Preliminary Results from Instrumentation Needs for *In Vivo* Counting in a Low-Background Underground Counting Facility. *Radiat. Prot. Dosimetry* 157 (1), 6–10. doi:10.1093/rpd/nct109

Sahu, P., Panigrahi, D. C., and Mishra, D. P. (2016). A Comprehensive Review on Sources of Radon and Factors Affecting Radon Concentration in Underground Uranium Mines. *Environ. Earth Sci.* 75 (7). doi:10.1007/s12665-016-5433-8

Scheler, R., Dettmann, K., and Brose, J. (1998). Retrospective Estimation of Exposure to Short-Lived 222Rn Progeny by Measurements of 210Pb in the Skull. *Radiat. Prot. Dosimetry* 79 (1-4), 129–132. doi:10.1093/oxfordjournals.rpd.a032375

Semkow, T. M., Parekh, P. P., Schwenker, C. D., Khan, A. J., Bari, A., Colaresi, J. F., et al. (2002). Low-background Gamma Spectrometry for Environmental Radioactivity. *Appl. Radiat. Isot.* 57 (2), 213–223. doi:10.1016/s0969-8043(02)00085-4

Somlai, J., Hakl, J., Kávási, N., Szeiler, G., Szabó, P., and Kovács, T. (2011). Annual Average Radon Concentration in the Show Caves of Hungary. *J. Radioanal. Nucl. Chem.* 287 (2), 427–433. doi:10.1007/s10967-010-0841-9

Sun, L., Wang, X. C., Pan, Y., Cui, H. X., Wu, Y. Y., and Liu, J. X. (2020). Investigation and Analysis of Radon Concentration in a Mining Area in Yunnan Province. *Chin. J. Radiol. Health* 29 (1), 57–60. doi:10.13491/j.issn.1004-714X.2020.01.013

Tomasek, L. (2020). Lung Cancer Lifetime Risks in Cohort Studies of Uranium Miners. *Radiat. Prot. Dosim.* 191 (2), 171–175. doi:10.1093/rpd/ncaa143

Turko, J., Pillalamarri, I., and Jagam, P. (2020). GEANT4 Simulations of Cosmic Muon Background in CEMRC BEGe Lung Detectors and Detection Sensitivity Optimization of Trans-uranic Radionuclides. *J. Radiat. Res. Appl. Sci.* 13 (1), 111–120. doi:10.1080/16878507.2019.1711341

UNSCEAR (2019). *UNSCEAR 2019 Report. Annex B: Lung Cancer from Exposure to Radon*. New York: United Nations: UNSCEAR.

Verplancke, J. (1992). Low Level Gamma Spectroscopy: Low, Lower, Lowest. *Nucl. Instrum. Meth. A.* 312 (1), 174–182. doi:10.1016/0168-9002(92)90149-X

Wahl, W., Haninger, T., Kucheida, D., Roth, P., and Paretzke, H. G. (2000). Study of Long-Term Radon Progeny in Humans for Retrospective Evaluation of Radon Exposure. *J. Radioanal. Nucl. Ch.* 243 (2), 447–450. doi:10.1023/A:1016078115609

WHO (2009). *WHO Handbook on Indoor Radon: A Public Health Perspective*. Geneva: World Health Organization.

Zheng, R. Q., Wang, S. L., Ma, R. W., Pan, Y. G., Jin, Y. R., Li, Y. Y., et al. (1992). Skull ^{210}Pb Content Measurement and Lung Dose Estimation from Radon Progeny of Tin Miners. *Radiat. Prot. Bull.*, 45–53.

Conflict of Interest: The authors declare that the research was conducted in the absence of any commercial or financial relationships that could be construed as a potential conflict of interest.

Publisher's Note: All claims expressed in this article are solely those of the authors and do not necessarily represent those of their affiliated organizations, or those of the publisher, the editors and the reviewers. Any product that may be evaluated in this article, or claim that may be made by its manufacturer, is not guaranteed or endorsed by the publisher.